



**HAL**  
open science

## Precipitation Process of Calcium Phosphate from Calcium Carbonate Suspension

Nayane Macedo Portela Da Silva, Fabienne Espitalier, Ange Nzihou

► **To cite this version:**

Nayane Macedo Portela Da Silva, Fabienne Espitalier, Ange Nzihou. Precipitation Process of Calcium Phosphate from Calcium Carbonate Suspension. *KONA Powder and Particle Journal*, 2016, 33, pp.219-227. 10.14356/kona.2016002 . hal-01620289

**HAL Id: hal-01620289**

**<https://hal.science/hal-01620289>**

Submitted on 5 Sep 2018

**HAL** is a multi-disciplinary open access archive for the deposit and dissemination of scientific research documents, whether they are published or not. The documents may come from teaching and research institutions in France or abroad, or from public or private research centers.

L'archive ouverte pluridisciplinaire **HAL**, est destinée au dépôt et à la diffusion de documents scientifiques de niveau recherche, publiés ou non, émanant des établissements d'enseignement et de recherche français ou étrangers, des laboratoires publics ou privés.

# Precipitation Process of Calcium Phosphate from Calcium Carbonate Suspension<sup>†</sup>

Nayane Macedo Portela da Silva, Fabienne Espitalier\* and Ange Nzihou

<sup>1</sup> Université de Toulouse, Centre RAPSODEE UMR CNRS 2392, France

## Abstract

The Ca-HA is synthesized by reacting calcium carbonate ( $\text{CaCO}_3$ ) and ammonium dihydrogen orthophosphate ( $\text{NH}_4\text{H}_2\text{PO}_4$ ) in stoichiometric proportions. In this precipitation process, the ratio of Ca/P by moles is 1.67. The experiments were performed in a batch reactor at 25 °C. From control parameters, the pH and the temperature were measured in line for all experiments. The tests were performed with two liquid-solid mass ratios ( $\text{H}_2\text{O}/\text{CaCO}_3$ ) of 3 and 5. For each mass ratio, three stirring rates of 260, 400, and 600 rpm were tested. Samples of the synthesis were collected at different intervals and analysed by laser granulometry and by environmental scanning electron microscopy.

For the synthesis conducted at 260 rpm, synthesis monitoring was made using a contact probe in solution coupled to a Raman spectrometer in order to follow the formation of solid phase. This technique is valuable to follow the synthesis of Ca-HA in a concentrated solids suspension (around 20–30 wt%).

The results make it possible to propose a mechanism of the precipitation process of Ca-HA. It can be divided into four main stages: (i) dissolution of calcium carbonate ( $\text{CaCO}_3$ ), (ii) precipitation of brushite ( $\text{CaHPO}_4 \cdot 2\text{H}_2\text{O}$ ), (iii) transformation of brushite into Ca-HA ( $\text{Ca}_{10}(\text{PO}_4)_6(\text{OH})_2$ ) and (iv) nucleation, growth and agglomeration of Ca-HA.

**Keywords:** precipitation, hydroxyapatite, brushite, Raman spectroscopy

## 1. Introduction

The exponential population growth has led to a similar increase in requirements for resources, energy, food, housing and land as well as an enormous increase in industrialization and urbanization. This rapid industrialization and urbanization have led to great demand for natural resources and created an increase in waste production. A continuing issue facing society today is the disposal of municipal and industrial wastes (Wey et al., 2006). Waste calcium carbonate ( $\text{CaCO}_3$ ) from the paper, cosmetics, pharmaceuticals, catalyst, ceramics, rubber and paint industries often ends up in landfill (Wen et al., 2007). These  $\text{CaCO}_3$  wastes can be used as the calcium compound in the synthesis of hydroxyapatite (Ca-HA). Ca-HA,  $\text{Ca}_{10}(\text{PO}_4)_6(\text{OH})_2$ , is an insoluble calcium phosphate mineral. It is a main constituent of bones and teeth. Due to its excellent biocompatibility, slow biodegradation, good mechanical stability, great sorption properties and heteroge-

neous photocatalytic degradation under UV irradiation (Wang et al., 2003), it has been used extensively for bone repairs, bone implants, bioactive materials and for purification and separation of biological molecules and organic contaminants. It can accept a series of cationic and anionic substitution within its structure (Elliott, 1994). Similarly, it has been reported to be an efficient adsorbent to treat heavy metals (Chen et al., 1997) and to have a very high capacity for removing divalent heavy metal ions (Ma et al., 1993). Consequently, hydroxyapatite is used for the removal of heavy metals from contaminated soils, wastewater and fly ashes (Elliott, 1994). Several methods have been developed to prepare Ca-HA, including a dry process, precipitation, hydrolyzation of calcium phosphate and hydrothermal synthesis. Spray pyrolysis, freeze drying, gel diffusion, a sol-gel technique and electrochemical deposition have all also been used. Much work has been done on the synthesis of Ca-HA using different methods such as solid-solid reaction (Nakamura et al., 2001; Silva et al., 2003), ultrasonic spray freeze-drying (Itatani et al., 2000) or spray-drying techniques generating a Ca-HA powder of controlled morphology (Luo and Nieh, 1996), sol-gel technique (Anee et al., 2003; Bezzi et al., 2003; Salimi et al., 2012), precipitation in aqueous solution (Jarcho, and Bolen, 1976; Rodriguez-Lorenzo et al., 2001; Bailliez and Nzihou, 2004; Swain et al., 2012), emulsion

<sup>1</sup> Ecole des Mines d'Albi-Carmaux, Campus Jarlard F-81013 Albi Cedex 09, France

\* Corresponding author: Fabienne Espitalier;  
E-mail: fabienne.espitalier@mines-albi.fr  
TEL: + 33-5-63493151 FAX: + 33-5-63493025

route (Saha et al., 2009; Okada et al., 2012), microwave-assisted synthesis (Ipekoglu and Altintas, 2010) and synthesis under hydrothermal conditions (Vasile et al., 2012; Murakami et al., 2012). Among all these methods, precipitation is characterized by the simplicity of the process, its low cost and its easy application in industrial production (Liu et al., 2001). The main objective of this work is to investigate this synthesis of calcium phosphate powders to be used as adsorbents for pollutants removal. To achieve this goal, the hydroxyapatite is synthesized by a crystallization reaction (precipitation) from solid calcium carbonate in a batch reactor in order to investigate systematically the effects of operating conditions such as the stirring speed and the liquid-solid mass ratios. These parameters determine the crystallization performance. Moreover in this study we show that the solid formations can be followed using Raman spectroscopy.

## 2. Experimental section

### 2.1 Materials and methods

In order to synthesize Ca-HA, laboratory-grade calcium carbonate ( $\text{CaCO}_3$ ) powder (98 % pure) and ammonium dihydrogen orthophosphate powder ( $\text{NH}_4\text{H}_2\text{PO}_4$ ) (94.4 % pure) were used. Both were obtained from Fisher Scientific U.K. and were used as received. The suspension of  $\text{CaCO}_3$  was introduced into a 0.5 L glass vessel (diameter 10 cm) with double jacket equipped with a helicoidal stirrer (diameter 4.5 cm). Agitation was powered by a Eurostar IKA laborotechnick 2000 motor. The reactor was equipped with four baffles (Fig. 1). The  $\text{NH}_4\text{H}_2\text{PO}_4$  powder was dissolved for a minimum time of 30 min at ambient temperature. Then, this solution was gradually pumped into the reactor with a peristaltic pump (Master

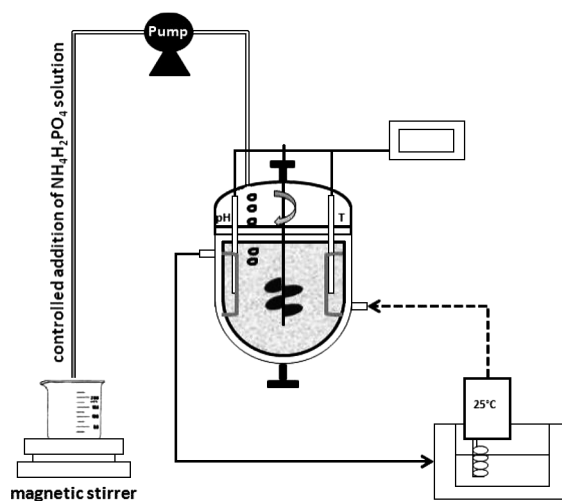


Fig. 1 Experimental set-up for precipitation.

flex pump) at a flow rate of  $11.11 \text{ cm}^3/\text{min}$  in order to maintain the pH value higher than 7. The temperature was controlled by a water bath (Julabo VC F30). The pH value was monitored throughout the duration of the experiment using a pH meter (Meterlab PHM210). The reaction continued for 72 h at atmospheric pressure and temperature ( $25 \pm 2 \text{ }^\circ\text{C}$ ). The ratio of Ca/P by moles was 1.67. Two different liquid-solid mass ratios (water/ $\text{CaCO}_3$  solid) of 3 and 5 and three stirring rates (260, 400 and 600 rpm) were tested. Addition times were equal to 18.6 min and 18.0 min, respectively, for a mass ratio of 3 and 5.

### 2.2 Analytical methods

The reactor suspension, composed of calcium carbonate and calcium phosphates, was sampled at different intervals in order to characterize the solid and the solution.

**Particle-size distributions:** The particle size distributions were measured by laser diffraction with a Malvern Master Sizer 2000 instrument covering a size range of 0.1–2000  $\mu\text{m}$ . Suspension samples were diluted and dispersed in water by ultrasonication for 4 min before measurement to disaggregate the solid. Direct sampling of the reactor suspension was used for these measurements.

For the other analysis, the collected samples were filtered. Solids were washed and dried in a vacuum oven (Heraeus Vacutherm—VT-6025) at  $60 \text{ }^\circ\text{C}$  for 24 hours to yield a fine white powder. The dry solid was not very cohesive and it was simply broken up by manual grinding.

Ion chromatography was used to analyse the liquid, and TG-DSC and ESEM for the solids.

**Ion phosphate concentration:** The phosphate ion concentration was analysed using ion chromatographic separation and it is performed using a Dionex ICS-300 ion chromatograph system consisting of: a single pump (Dionex ICS-3000 SP), an eluent generator (Dionex ICS-3000 EG), a conductivity detector (Dionex Conductivity Detector P/N 061830), a precolumn (Dionex IonPac AG 19,  $4 \times 50 \text{ mm}$ ) and a column (Dionex IonPac AS 19 ( $4 \times 250 \text{ mm}$ )). The eluent was the ultra-pure water with the pH value kept constant by using the KOH eluent generator. The eluent flow was 1 ml/min corresponding to a stable pressure in the column of about 120 bar. The results were analysed by using the software Chromelon.

**Habitus:** A scanning electron microscope (Philips XL30 ESEM FEG) equipped with EDAX fluorescence analysis following platinum sputtering of the sample, was used to study the morphology of the gold-coated intermediate and final products.

**Weight losses:** Thermal gravimetric analysis was performed using a Thermogravimetric Analyser (TGA-DSC 111 Setaram). The experiment was performed with a heating rate of  $2 \text{ }^\circ\text{C}/\text{min}$  using nitrogen flow ( $25 \text{ ml}/\text{min}$ ). The percentage weight loss of the samples (approximately

12 mg) was monitored from 20 to 800 °C.

**Raman spectra:** For the synthesis conducted at 260 rpm, the synthesis monitoring was conducted using a contact probe in solution coupled to a Raman spectrometer RXN2C785, Mettler-Toledo/Kaiser analysers (Kaiser Optical Systems, Ann Arbor, Michigan, USA). A 400 mW external cavity stabilized by an Invictus NIR diode laser at 785 nm was used for sample illumination. All the spectra were recorded at a resolution of 4 cm<sup>-1</sup>.

**XR diffraction:** For the synthesis conducted at 260 rpm, the phase identification of some samples was carried out using XR diffractometry (Phillips PanAlytical X'Pert Pro MPD diffractometer), which had a Cu Ka radiation ( $\lambda = 1.54 \text{ \AA}$ ) at 45 kV and 40 mA. The reflections were collected in the  $2\theta$  ranges from 10 to 75° with a step size of 0.17° and a time of 13.02 s per step. The phase identification was carried out with the JCPDS database.

### 3. Results

During the process for the formation of hydroxyapatite, it was possible to form other calcium phosphates. Their solubilities decrease with the pH value (Ferreira et al., 2003). The comparisons of the solubility of the CaHPO<sub>4</sub>·2H<sub>2</sub>O named brushite and the solubility of hydroxyapatite Ca-HA for a pH value lower than 4, show that brushite is a stable compound and for a pH value higher than 4, the Ca-HA is prominent. **Fig. 2** shows the evolution of the pH value during the synthesis for the two liquid-solid mass ratios (3 and 5) at 400 rpm. It can be observed that the pH value readily decreases from 10.2 to 6.9 during the first 15 minutes of reaction. Then it gradually increases to 8.5 and after 40 hours, the pH value stabilizes at about 9. The liquid-solid mass ratio does not influence the pH value.

At 25 °C in the pH range [8-9] (**Fig. 2**), it was possible to form three solids: the monetite (CaHPO<sub>4</sub>), the brushite (CaHPO<sub>4</sub>·2H<sub>2</sub>O) and the hydroxyapatite (Ca<sub>10</sub>(PO<sub>4</sub>)<sub>6</sub>(OH)<sub>2</sub>).

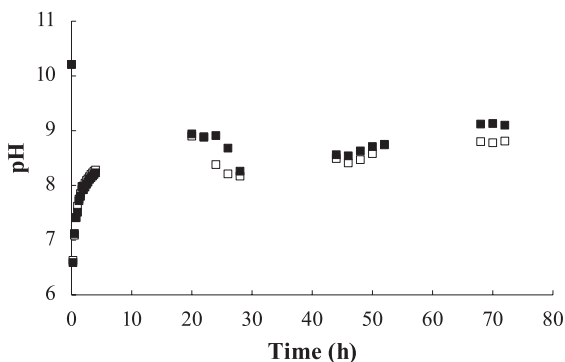


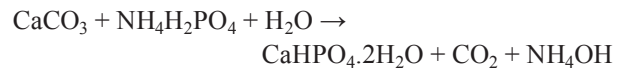
**Fig. 2** Evolution of the pH value during synthesis at 400 rpm for two mass ratios (3 □ and 5 ■).

Their formation follows these three reactions respectively (Chkir, 2011; Verwilghen, 2009):

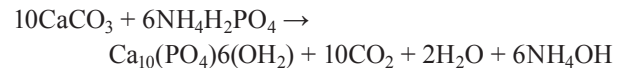
(1) Monetite (metastable phase):



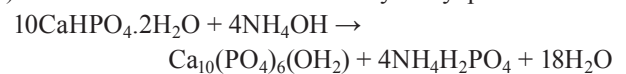
(2) Brushite:



(3) Hydroxyapatite:



(4) Transformation of brushite into hydroxyapatite



The analysis did not detect monetite.

When any amount of ammonium dihydrogen phosphate is introduced into the reactor containing the calcium carbonate suspension, gas bubbles with an ammonium odor are observed. This confirms the formation of carbon dioxide and ammonium during the reaction.

As the pH showed low values at the beginning of the synthesis, this may have favored the formation of brushite. The end of synthesis, which sees the stabilization of the pH value at around 9, favors the formation of hydroxyapatite.

#### 3.1 Influence of mass ratio

Two syntheses with two liquid-solid mass ratios of 3 and 5, respectively, carried out at a low stirring rate of 260 rpm in the presence of a RAMAN probe to study the influence of this ratio on the synthesis of Ca-HA.

Tsuda and Arends (1993) give the Raman bands observed for three pure minerals (brushite, octacalcium phosphate OCP and Ca-HA). The spectral features of solids can be characterized as Raman bands due to phosphate (PO<sub>3</sub><sup>4-</sup>) vibrational modes of  $\nu_4$ ,  $\nu_2$ ,  $\nu_1$  and  $\nu_3$ . The intensity of the  $\nu_1$  band is the strongest, and can be used for the identification of minerals.

**Figs. 3, 4 and 5** show the Raman spectra during the synthesis made with a mass liquid-solid ratio of 5 and a stirring rate of 260 rpm. In **Fig. 3**, we observe the appearance of a peak at 983 cm<sup>-1</sup> after 20 min of synthesis. This peak is relatively wide. Its intensity increases with time. This peak noted on **Fig. 4** corresponds to the brushite, a compound observed in previous studies (Chkir, 2011).

The presence of brushite is confirmed by XR diffraction analysis (**Fig. 6**).

After 19 h, a second peak close to the brushite peak appears at 962 cm<sup>-1</sup>; this corresponds to the Ca-HA. While the peak intensity of brushite decreases, the peak inten-

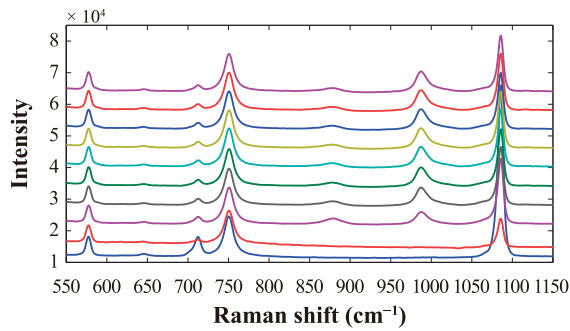


**Fig. 3** Raman spectra measured every 19 min between 0 and 3 h, (liquid-solid mass ratio = 5 and  $N = 260$  rpm). Times from the bottom to the top.

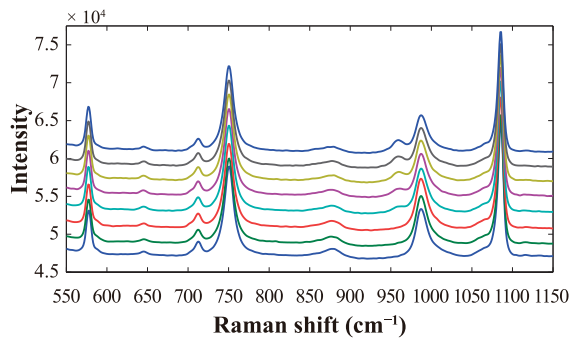


**Fig. 4** Raman spectra measured every 4 h between 3 h 10 min and 24 h 19 min, (liquid-solid mass ratio = 5 and  $N = 260$  rpm). Times from the bottom to the top.

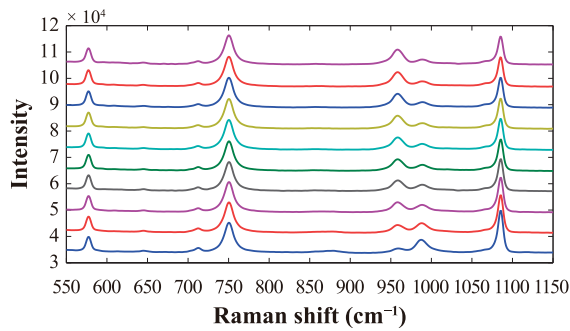


**Fig. 5** Raman spectra measured every 8 h between 19 h 20 min and 91 h 20 min, (liquid-solid mass ratio = 5 and  $N = 260$  rpm). Times from the bottom to the top.

sity of Ca-HA increases (**Figs. 4 and 5**). After 30 h, the intensities of all peaks are stable. This assumption has been verified qualitatively by XR diffraction analysis (**Fig. 7**). At 44 h, the brushite is no longer visible by this technique. The large peak observed at 30–33° corresponds to Ca-HA.

**Fig. 8** shows the weight losses of the different samples measured between 20 and 800 °C by TG analysis for dry solids obtained during the synthesis made with a mass ratio of 5 and a stirring rate of 260 rpm. For the pure cal-

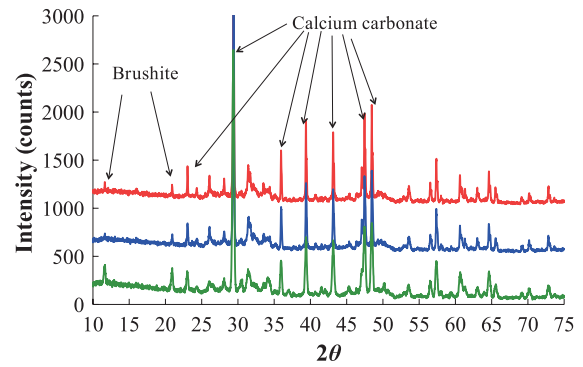


**Fig. 6** XR diffraction spectra at 0.75, 2 and 4 hours (liquid-solid mass ratio = 5 and  $N = 260$  rpm). Times from the bottom to the top.

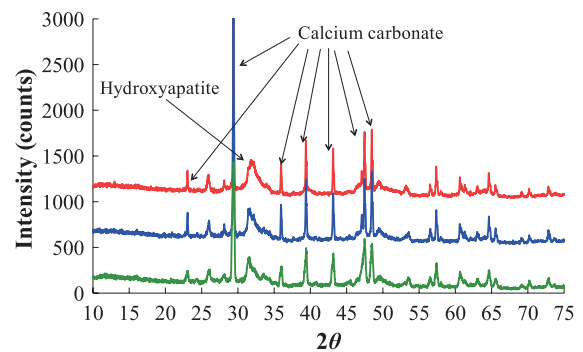


**Fig. 7** XR diffraction spectra at 44, 50 and 68 hours (liquid-solid mass ratio = 5 and  $N = 260$  rpm). Times from the bottom to the top.

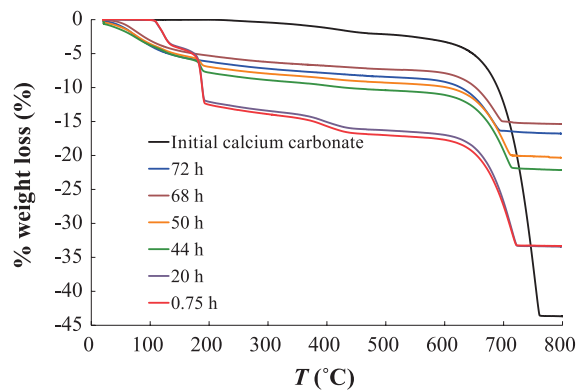


**Fig. 8** Weight losses between 20 and 800 °C at 0, 0.75, 4, 20, 44, 50, 68 and 72 h (liquid-solid mass ratio = 5 and  $N = 260$  rpm).

cium carbonate, two weight losses are observed: one between 350 and 400 °C and another after 600 °C. The first loss is due to the degradation of impurities contained in  $\text{CaCO}_3$ . The decomposition of calcium carbonate ( $\text{CaCO}_3$ ) in calcium oxide ( $\text{CaO}$ ) and carbon dioxide ( $\text{CO}_2$ ) (decarbonation) induces the second loss.

For the other samples, three weight losses are observed.

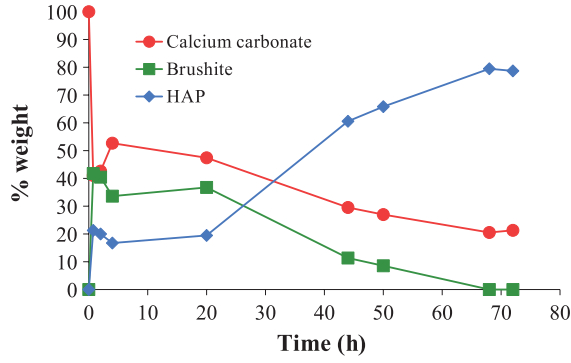


**Fig. 9** Mass percentages of brushite, calcium carbonate and Ca-HA during the synthesis.

The first is between 180 and 200 °C, the second between 350 and 400 °C and the third after 600 °C. This first is attributed to loss of the hydration water of brushite (detected by RAMAN spectra analysis), the second to impurities and the third to the decarbonation of unreacted  $\text{CaCO}_3$ . The weight loss observed between 50 and 120 °C is due to insufficient drying of these samples. From these mass losses, by assuming that only three solids are present in the reactor ( $\text{CaCO}_3$ ,  $\text{CaHPO}_4 \cdot 2\text{H}_2\text{O}$  and  $\text{Ca}_{10}(\text{PO}_4)_6(\text{OH})_2$ ), the mass percentage of these three components in the solid can be calculated (**Fig. 9**).

Four steps can be observed. The first step (I) corresponds to the dissolution of calcium carbonate and formation of apatite: a sharp decrease in calcium carbonate (around 40 %) during the first hour, and a sharp increase in brushite (around 40 %) and Ca-HA (around 20 %).

During the second step (II) between 4 and 20 h, the weight percentage of solids seems to be constant. After 20 h, we can observe an increase in the weight percentage of Ca-HA up to 80 wt% and a decrease in the  $\text{CaCO}_3$  and brushite weight percentages. This step (III) corresponds to the transformation of brushite into Ca-HA by dissolution-crystallization or by solid-solid transformation. However, the reaction is not complete and 20 wt% of the solid remaining is composed of calcium carbonate. After 68 h, two solids are in suspension:  $\text{CaCO}_3$  and Ca-HA. The mass balance on calcium leads to the total weight as a function of time from mass fractions and initial weight of  $\text{CaCO}_3$ :

$$m_T(t) = \frac{m_{\text{CaCO}_3}^i}{M_{\text{CaCO}_3}} \frac{1}{\left( \frac{w_{\text{brushite}}}{M_{\text{brushite}}} + 10 \frac{w_{\text{HAP}}}{M_{\text{HAP}}} + \frac{w_{\text{CaCO}_3}}{M_{\text{CaCO}_3}} \right)} \quad (1)$$

where  $m_{\text{CaCO}_3}^i$  is the initial weight of  $\text{CaCO}_3$ ,  $M_j$  the molar weight and  $w_j$  the mass fraction of the component  $j$  in the solids mixture.

**Fig. 10** presents the evolution of weight of each solid during a synthesis for both liquid-solid mass ratios, 3 and 5.

Furthermore, by coupling the results of the loss of mass

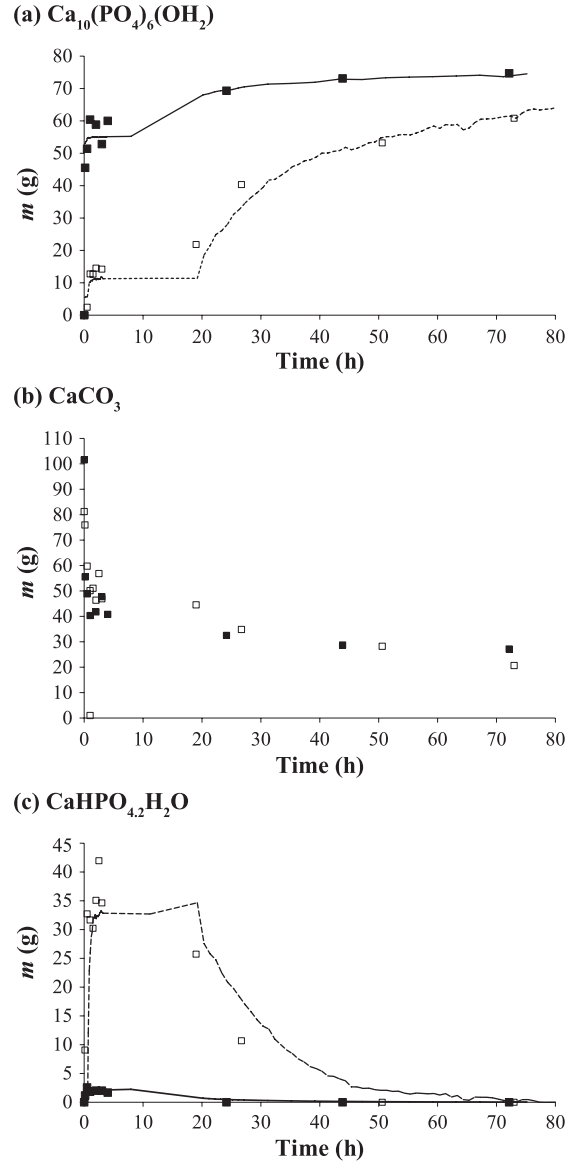


**Fig. 10** Masses during the synthesis ( $N = 260$  rpm) for liquid-solid mass ratio = 5, symbols: hollow square and - -; and liquid-solid mass ratio = 3, symbols: black square and - .

and the RAMAN spectra, it is possible to calibrate the area of RAMAN peaks observed in 983 and 962  $\text{cm}^{-1}$ , respectively, for the brushite and the Ca-HA according to the mass fractions obtained by TGA. This calibration leads to the continuous curves given in **Fig. 10**. Both weight ratios lead to final masses that are close to  $\text{CaCO}_3$  initial masses.

The conversion does not seem to depend on the initial weight ratio. This conversion is not total, but is of the order of 73–74 wt%. We also note that the maximum mass of brushite formed for a liquid-solid mass ratio equal to 3 is 13 times weaker than that formed for a liquid-solid mass ratio of 5 (**Fig. 10 (c)**).

Beyond 20 h for a liquid-solid ratio of 3 and 40 h for a

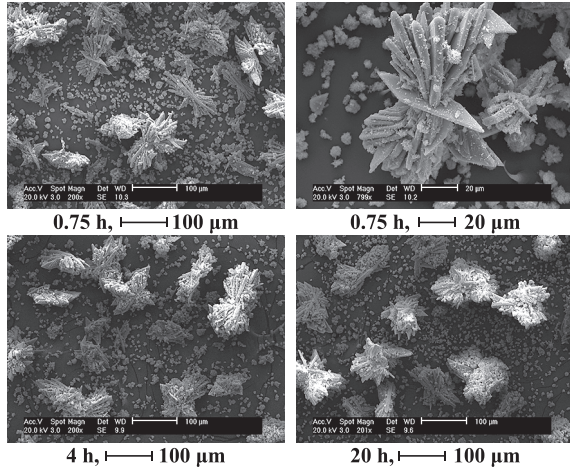


**Fig. 11** Morphology of brushite at 0.75, 4 and 20 h (liquid-solid mass ratio = 5 and  $N = 260$  rpm).

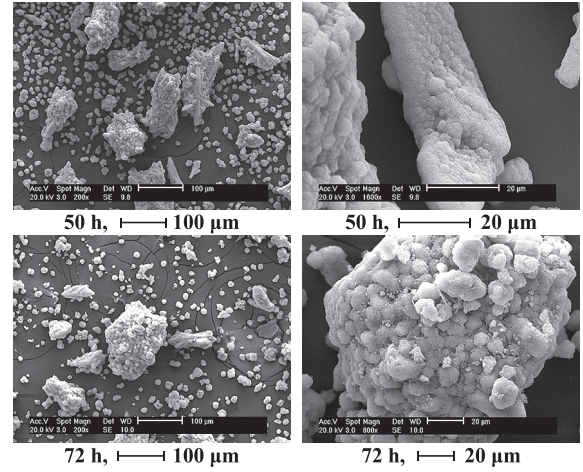


**Fig. 13** Morphology of Ca-HA 50 and 72 h (liquid-solid mass ratio = 5 and  $N = 260$  rpm).

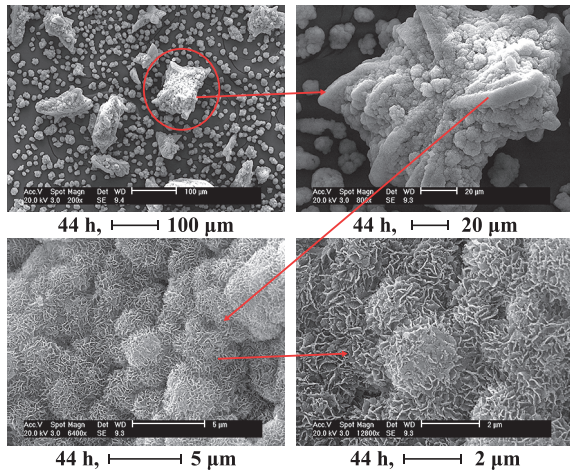


**Fig. 12** Morphology of Ca-HA at 44 h (liquid-solid mass ratio = 5 and  $N = 260$  rpm).

liquid-solid ratio of 5, the brushite seems to have totally disappeared. In parallel, the formation of Ca-HA is much faster for an  $L/S$  ratio of 3 within the first hours (77 wt% of the final mass is reached (**Fig. 10 (a)**). After 10 h of synthesis, a slowing down is observed.

The particles of brushite are formed preferably in the solution (**Fig. 11**), while the particles of Ca-HA are created on the surface of the brushite particles (**Fig. 12**) or (**Fig. 11**). The particles of  $\text{CaCO}_3$  are attacked by orthophosphate ions. Therefore,  $\text{CaCO}_3$  is used to form monentite. This compound is transformed into brushite which evolves to the hydroxyapatite (calcium phosphate thermodynamically more stable). When the liquid-solid mass ratio decreases, the available surface of  $\text{CaCO}_3$  is larger, allowing the reaction (3) to occur on the surface of  $\text{CaCO}_3$ . This behavior limits the brushite formation by reaction (2). The mass growth rate of Ca-HA at the initial time can be written as:

$$\left. \frac{dm_{\text{Ca-HA}}}{dt} \right|_{t=0} = K S^j \Delta C^g \quad (2)$$

where  $K$  is a kinetic constant,  $\Delta C$  is the absolute supersaturation of Ca-HA, and  $S$  is the  $\text{CaCO}_3$  disposable surface at the time at which Ca-HA is detectable.

As the initial size distribution of calcium carbonate is identical, the surface ( $S$ ) is assumed proportional to mass.

The ratio of these initial rates for liquid-solid mass ratios of 3 and 5 leads to a coefficient  $j$  of the order of 12.5, thereby showing a strong influence of the available surface of calcium carbonate on the Ca-HA formation. As the Ca-HA layer forms on the surface of  $\text{CaCO}_3$ , the diffusion of orthophosphate and calcium ions is limited thus reducing the mass growth formation of Ca-HA observed beyond 10 h for a liquid-solid mass ratio of 3. In the case of a higher ratio, it can be assumed that reactions (2) and (4), which represent the  $\text{CaCO}_3$  and brushite formations, respectively, occur in parallel.

**Fig. 14** shows the evolution of the mass mean diameter as a function of the time based on both mass ratios (liquid-solid mass ratios of 3 and 5) for a stirring speed of 260 rpm. For a liquid-solid mass ratio of 5, the increase in average diameter (7–22 microns) between 0 and 3 is due to the brushite formation (**Fig. 14 (a)**). After 3 h, the mean diameter decreases assumed by brushite dissolution. Beyond 20 h, the mean diameter increases following the same trend as Ca-HA mass (**Fig. 14 (b)**).

Brushite dissolution allows Ca-HA formation. This compound is thermodynamically more stable than brushite (Ferreira et al. 2003) and it forms on the surface of  $\text{CaCO}_3$  causing the increase in diameter. For a liquid-solid mass ratio of 3 (**Figs. 15 (a) and (b)**), the same behavior is observed, meaning that the mass mean diameter increases, then decreases and finally increases again. However, beyond 20 h, the mean diameter does not change (about 20  $\mu\text{m}$ ) because the Ca-HA mass stabilizes.

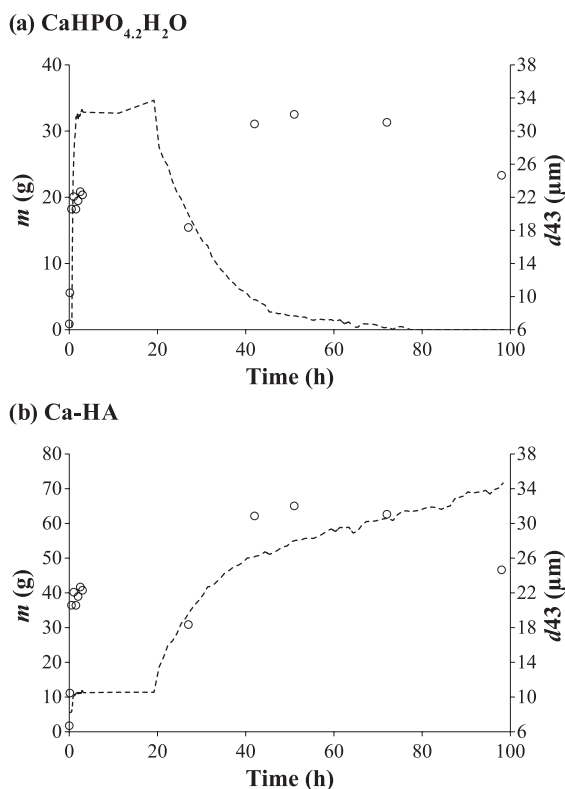


**Fig. 14** CaHPO<sub>4</sub>.2H<sub>2</sub>O and Ca-HA masses calculated from RAMAN spectra and mean volume diameter during synthesis ( $N = 260$  rpm and liquid-solid mass ratio = 5), symbols: hollow circle ( $d_{43}$ ) and -- (compound masses).

**Fig. 16** presents the mean diameters of the particles during synthesis for different stirring speeds (400 and 600 rpm) for both mass ratios ( $L/S = 3$  and 5). The results obtained at 400 and 600 rpm show the same behavior obtained at 260 rpm (increase, decrease, re-increase and stabilization of mean diameter). After 40 h of synthesis, the measured diameters are identical ( $23 \pm 1 \mu\text{m}$ ) for a stirring speed equal to 400 rpm (**Fig. 16 (a)**). Larger agglomerates are observed at a low stirring speed after 72 h of synthesis. The stabilization of the mean diameter is observed after 40 h for all the syntheses except for the synthesis performed at 600 rpm. In this case after 20 h of synthesis, the mass mean diameter is stable and equals  $16 \pm 1 \mu\text{m}$  (**Fig. 16 (b)**).

#### 4. Conclusions

In this study, we show that Raman spectroscopy is a valuable technique to follow the synthesis of Ca-HA in a concentrated solids suspension (around 20–30 wt%). This technique makes it possible to follow the formation of Ca-HA and brushite and to deduce from complementary measurements a formation mechanism described as fol-

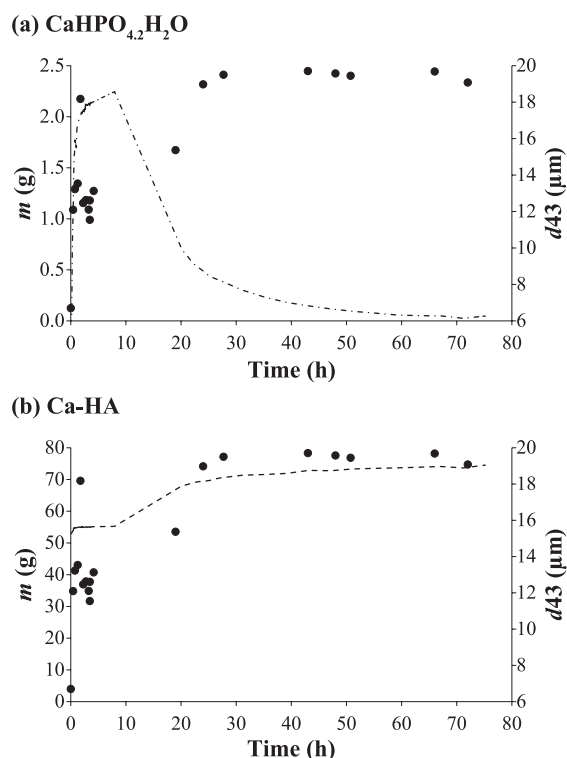


**Fig. 15** CaHPO<sub>4</sub>.2H<sub>2</sub>O and Ca-HA masses calculated from RAMAN spectra and mean volume diameter during synthesis ( $N = 260$  rpm and liquid-solid mass ratio = 3), symbols: black circle ( $d_{43}$ ) and -- (compound masses).

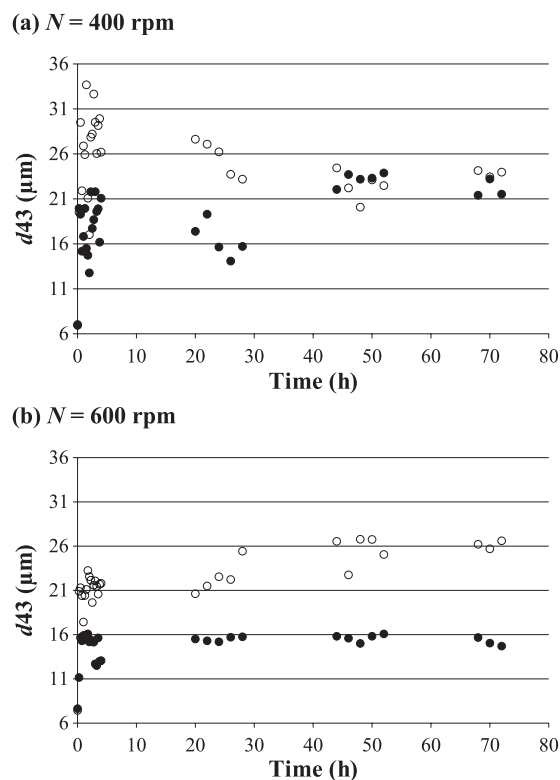


**Fig. 16** Mean volume diameter during the synthesis, symbols: black circle (liquid-solid mass ratio = 3) and hollow circle (liquid-solid mass ratio = 5).

lows:

- The dissolution of calcium carbonate is observed in the first minutes of synthesis.
- The precipitation of brushite and Ca-HA particles is observed in the first four hours of synthesis.
- The transformation of brushite into hydroxyapatite begins after one day. It seems to be the limiting step.

In terms of morphology, agglomerates of hollow ellipsoidal particles were obtained corresponding to the calcium carbonate, while platelets agglomerated like stars corresponded to the brushite and agglomerated spongy spheres or round stick-like compounds of spongy spheres corresponded to the hydroxyapatite.

Through the mass balance obtained from thermogravimetric analysis and from the phosphate ions, it was also verified that at the end of the synthesis, the calcium carbonate was not completely consumed.

Therefore, the reaction is not complete at the end of the synthesis (72 h).

From the analysis performed by laser granulometry during the synthesis with a mass equal to five and three at 260, 400 and 600 rpm, there was a strong influence of the stirring speed on the process. The two effects (positive and negative) that explain the agglomeration process have been presented. For the synthesis with a mass ratio equal to five, the first effect called the size-enlargement phenomenon predominated. In contrast, for the synthesis with a mass ratio equal to three, a predominance of the second effect called the breakage phenomenon was observed. These phenomena were confirmed by the observations made using the environmental electron microscopy of the synthesized solids.

## 5. Acknowledgements

The authors would like to thank M. H. Lucas for support in the data analysis of RAMAN spectra. They also thank Ms S. Del Confetto, Ms C. Rolland, Ms N. Lyczko and M.P. Accart, respectively, for TG measurements, microscopy analysis and X-Ray, and particle size analysis.

## References

- Anee T.K., Ashok M., Palanichamy M., Kalkura S.N., A novel technique to synthesize hydroxyapatite at low temperature, *Materials Chemistry and Physics*, 80 (2003) 725–730.
- Bailliez S., Nzihou A., The kinetics of surface area reduction during isothermal sintering of hydroxyapatite adsorbent. *Chemical Engineering Journal*, 98 (2004) 141–152.
- Bezzi G., Celotti G., Landi E., La Torretta T.M.G., Sopyan I., Tampieri A., A novel sol–gel technique for hydroxyapatite preparation. *Materials Chemistry and Physics*, 78 (2003) 816–824.
- Chen X., Wright J.V., Conca, L.M., Peurrung J.L., Effects of pH on heavy metal sorption on mineral apatite. *Environmental Science and Technology*, 31 (1997) 624–631.
- Chkir M., Synthèse de gels phosphocalciques issus de déchets industriels carbonates. Caractérisation physico-chimique, thermique et rhéologique. PhD thesis, Thèse de l'Université de Toulouse Institut National Polytechnique de Toulouse, 2011.
- Elliott J.C., *Structure and Chemistry of the Apatites and Other Calcium Orthophosphates*, Elsevier, Amsterdam, 1994.
- Ferreira A., Oliveira C., Rocha F., The different phases in the precipitation of dicalcium phosphate dihydrate, *Journal of Crystal Growth*, 253 (2003) 599–611.
- Itatani K., Iwafune K., Howell F.S., Aizawa M., Preparation of various calcium-phosphate powders by ultrasonic spray freeze-drying technique. *Materials Research Bulletin*, 35 (2000) 575–585.
- Ipekoglu M., Altintas S., Silver substituted nanosized calcium deficient hydroxyapatite. *Materials Technology: Advanced Performance Materials*, 25 (2010) 295–301.
- Jarcho M., Bolen C.H., Hydroxylapatite synthesis and characterization in dense polycrystalline form, *Journal of Materials Science*, 11 (1976) 2027–2035.
- Liu C., Huang Y., Shen W., Cui J., Kinetics of hydroxyapatite precipitation at pH 10 to 11, *Biomaterials*, 22 (2001) 301–306.
- Luo P., Nieh T.G., Preparing hydroxyapatite powders with controlled morphology, *Biomaterials*, 17 (1996) 1959–1964.
- Ma Q.Y., Traina S.J., Logan T.J., Ryan J.A., In situ lead immobilisation by apatite, *Environmental Science and Technology*, 27 (1993) 1803–1810.
- Murakami S., Kato K., Enari Y., Kamitakahara M., Watanabe N., Ioku K., Hydrothermal synthesis of porous hydroxyapatite ceramics composed of rod-shaped particles and evaluation of their fracture behaviour. *Ceramics International*, 38 (2012) 1649–1654.
- Nakamura S., Isobe T., Senna M., Hydroxyapatite nano sol prepared via a mechanochemical route. *Journal of Nanoparticle Research*, 3 (2001) 57–61.
- Okada M., Fujii S., Nishimura T., Nakamura Y., Takeda S., Furuzono T., Solvent-free formation of hydroxyapatite coated biodegradable particles via nanoparticle-stabilized emulsion route, *Applied Surface Science*, 262 (2012) 39–44.
- Rodriguez-Lorenzo L.M., Vallet-Regi M., Ferreira J.M.F., Fabrication of hydroxyapatite bodies by uniaxial pressing from a precipitated powder, *Biomaterials*, 22 (2001) 583–588.
- Saha S.K., Banerjee A., Banerjee S., Bose S., Synthesis of nanocrystalline hydroxyapatite using surfactant template systems: Role of templates in controlling morphology. *Materials Science and Engineering: C*, 29 (2009) 2294–2301.
- Silva C.C., Pinheiro A.G., Miranda M.A.R., Góes J.C., Sombra, A.S.B., Structural properties of hydroxyapatite obtained by mechanosynthesis, *Solid State Science*, 5 (2003) 553–558.
- Swain S.K., Dorozhkin S.V., Sarkar D., Synthesis and dispersion of hydroxyapatite nanopowders, *Materials Science and Engineering: C*, 32 (2012) 1237–1240.

- Tsuda H., Arends J., Raman spectra of human dental calculus, *Journal of Dental Research*, 72 (1993) 1609–1613.
- Vasile E., Popescu L.M., Piticescu R.M., Burlacu A., Buruiana T., Physico-chemical and biocompatible properties of hydroxyapatite based composites prepared by an innovative synthesis route, *Materials Letters*, 79 (2012) 85–88.
- Verwilghen C., Chkir M., Rio S., Nzihou A., Sharrock P., Depelsenaire G., Convenient conversion of calcium carbonate to hydroxyapatite at ambient temperature, *Materials Science and Engineering: C*, 29(3) (2009) 771–773.
- Wang C.X., Wang M., Zhou X., Nucleation and growth of apatite on chemically treated titanium alloy: an electrochemical impedance spectroscopy study, *Biomaterials*, 24 (2003) 3069–3077.
- Wen C.F., Zhao Y.L., Liang R.Z., Recycle of low chemical potential substance resources, *Conservation and Recycling*, 51 (2007) 475–486.
- Wey M.Y., Liu K.Y., Tsai T.H., Chou J.T., Thermal treatment of the y ash from municipal solid waste incinerator with rotary kiln, *Journal of Hazardous Material*, 137 (2006) 981–989.